Suitability of III-V $[XH_4][YH_4]$ materials for hydrogen storage: A density functional study

Filippo Zuliani,* Andreas W. Götz,† Célia Fonseca Guerra,‡ and Evert Jan Baerends§
Theoretische Chemie, Vrije Universiteit Amsterdam, De Boelelaan 1083, 1081 HV Amsterdam, The Netherlands
(Received 30 December 2008; revised manuscript received 25 February 2009; published 15 April 2009)

In the search for novel hydrogen storage media, the III-V hydridic material $[NH_4][BH_4]$ is a natural candidate. It can store a high wt % of hydrogen and has a favorable volumetric density. Unfortunately it was found to decompose slowly at room temperature. It is of interest to consider chemically related materials, such as the series of $[XH_4][YH_4]$ ionic solids (X=B,Al,Ga and Y=N,P,As). Even if the wt % of hydrogen in the heavier congeners is necessarily lower, they might offer superior material properties, notably higher (but not too high) stability. We have therefore performed a first-principles investigation of the cohesive energies of the XH_4YH_4 solid-state materials. In addition we have analyzed the bond character and energy within the building blocks of these materials, the XH_4^- and YH_4^+ molecular ions, including a comparison to the AH_4 molecules (A=C,Si,Ge). The calculations have been performed within the density functional framework employing plane waves for the bulk materials and Slater-type functions for the molecules. A detailed study of the electronic structure reveals that the hydrides of the light (second period) elements, BH_4^-, CH_4, and NH_4^+, exhibit the strongest and shortest X-H bonds. This is caused by Pauli repulsion effects of the hydrogen substituents with the larger cores of the heavier (third and fourth period) elements. The important consequence is that in the crystals, where the ionic hydrides retain their identity and charge, the distance between the negative and positive ions is larger in the heavier systems, hence less Madelung stabilization and a smaller cohesive energy. Moving from $[NH_4][BH_4]$ to heavier congeners thus does not seem to be a promising route to obtain more suitable materials for hydrogen storage. Other types of chemical variation (different substituents) on the $[NH_4][BH_4]$ building blocks may prove more advantageous.

DOI: 10.1103/PhysRevB.79.165106 PACS number(s): 61.50.Lt, 71.15.Nc, 71.15.Mb

I. INTRODUCTION

The development of a hydrogen economy promises clear economic, energetic, and environmental safety benefits. There is a critical need to develop new hydrogen storage materials and novel approaches for the release/uptake of hydrogen for use in on-board transportation systems.[1–4] An important step in this direction was the use of compounds containing B and N as hydrogen sources such as the ammonium borohydride salt NH_4.[5] Compared to the corresponding gaseous hydrocarbons,[6–8] the solid NH_4 provides far more favorable volumetric densities and is particularly interesting because of the large amount of hydrogen it stores (24.4 wt %). Unfortunately, it was found to be unstable, with 50% of sample decomposition after 6 h at room temperature.[5] The decomposition rate increases rapidly with temperature, thus preventing the use of NH_4 for hydrogen storage. A possible solution could be the employment of different III-V XH_4YH_4 materials, which still exhibit high wt % of stored hydrogen as shown in Table I.

Little is known about the XH_4YH_4 materials and NH_4 is the only one up to now that has been synthesized. A detailed characterization of crystal structure and the investigation of chemical properties is highly desirable, yet missing. Understanding the fundamental chemical properties of the complex hydrides is of central importance for the design of novel hydrogen storage materials and will likely be important to identify new viable candidates. We therefore investigate XH_4YH_4 (X=B,Al,Ga and Y=N,P,As) solid-state materials and their molecular building blocks composed by periodic arrays of XH_4^- and YH_4^+ molecular ions for hydrogen storage purposes. The paper is organized as follows. Computational details are given in Sec. II. In Sec. III, we investigate the X–H, A–H, and Y–H bond strength and character of the XH_4^- (X=B,Al,Ga), AH_4 (A=C,Si,Ge), and YH_4^+ (Y=N,P,As) molecules and molecular ions by means of population analysis and a Morokuma-type energy decomposition. In Sec. IV, we study the cohesive energies of different XH_4YH_4 materials in the most common salt structures present in nature (NaCl, CsCl, wurtzite, and zinc blende) by parameter-free methods and we provide a first estimate of the stability of the XH_4YH_4 solid-state materials. Our results are summarized in Sec. V.

II. COMPUTATIONAL DETAILS

All molecular calculations were performed with the Amsterdam density functional (ADF) program,[9–11] using the generalized gradient approximation (GGA) of density functional theory.[12] The molecular orbitals (MOs) were expanded in large sets of all-electron Slater-type functions (AOs) containing polarization functions of TZ2P quality. For the bond character analysis in the fragment approach (see Sec. III A) we used the DZ basis set of the ADF library. Equilibrium

TABLE I. wt % of stored hydrogen in different III-V XH_4YH_4 materials.

	NH_4	PH_4	AsH_4
BH_4	24.4	16.1	8.5
AlH_4	16.3	12.1	7.3
GaH_4	8.7	7.4	5.2

TABLE II. VDD charges (Q, a.u.) and electronegativity differences (Ref. 27) ($\Delta\chi=\chi_{X,A,Y}-\chi_H$, Pauling Units).

	XH_4^-				AH_4				YH_4^+		
	Q_X	Q_H	$\Delta\chi$		Q_A	Q_H	$\Delta\chi$		Q_Y	Q_H	$\Delta\chi$
B	−0.055	−0.236	−0.25	C	−0.091	0.023	0.25	N	−0.082	0.270	0.77
Al	0.233	−0.308	−0.69	Si	0.250	−0.062	−0.38	P	0.297	0.176	−0.05
Ga	0.196	−0.299	−0.54	Ge	0.227	−0.057	−0.31	As	0.303	0.174	−0.09

structures were optimized using analytical gradient techniques, with geometries and energies calculated at the Becke-Perdew[13,14] level of theory (BP86).

The solid-state calculations were performed using the ESPRESSO package.[15] Self-consistent density functional calculations were carried out in the local-density approximation (LDA) (Ref. 16) and generalized gradient approximation. For LDA we employed the exchange-correlation interaction in the parameterization given by Perdew and Zunger[17] with norm-conserving[18] pseudopotentials while for GGA the parameterization employed was from Perdew *et al.*[19] with ultrasoft[20] pseudopotentials. Wave functions were expanded in plane waves with energy cutoffs of 30 and 60 Ry for ultrasoft and norm conserving pseudopotentials, respectively, with a finite $\boldsymbol{k}$-points representation of the first Brillouin zone.[21–23] Electron densities, total energies, and atomic forces were calculated in a reciprocal-space formalism,[24,25] employing the Hellmann-Feynman theorem. All calculations were performed in the $(4\times4\times4)$ $\boldsymbol{k}$-points mesh of the irreducible wedge of the Brillouin zone. The effect of increasing the plane-wave cutoff from 30 to 40 Ry for ultrasoft calculations was to decrease the total energy by less than 10^{-3} eV for all considered systems, indicating a satisfactory convergence of the basis set. We also made test calculations with an $(8\times8\times8)$ $\boldsymbol{k}$-points mesh. Again, the result was a decrease in the total energy by less than 10^{-3} eV and very small ($<10^{-4}$ nm) changes of relaxed positions of atoms compared to the $(4\times4\times4)$ $\boldsymbol{k}$-points calculations.

III. XH_4^- AND YH_4^+ MOLECULAR BUILDING BLOCKS

A. Bond character

Understanding the fundamental chemical properties of the complex hydrides is of key importance for the design of novel hydrogen storage materials and will likely be important to identify new viable candidates. We begin our study of the bond character with an analysis of the effective atomic charges according to the Voronoi deformation density (VDD) method[26] as implemented in ADF, which has already proven to yield reliable results with only a small basis set dependency.[26] A standard method such as Mulliken charge analysis totally fails for these tetrahedral molecules; see Ref. 26.

The VDD method is based on the deformation density and a rigorous partitioning of space into nonoverlapping atomic areas, the so-called Voronoi cells. The VDD charge Q_A of an atom A is defined as the integral of the deformation density over the Voronoi cell of the atom [the part of space closer to that atom (nucleus) than to any other atom]. It reflects the change upon going from the promolecule, in which the density is the superposition of the initial, unperturbed atomic densities ρ_A, to the converged SCF density ρ of the molecule,

$$Q_A = \int_{\text{Voronoi cell } A} \left(\rho(\boldsymbol{r}) - \sum_B \rho_B(\boldsymbol{r})\right) d\mathbf{r}. \quad (1)$$

For neutral systems the VDD charges directly reflect the charge-density redistribution due to bond formation. For charged systems, when, as recommended, the neutral atoms are used to build the promolecule density, the VDD charges will sum up to the total charge of the system and will indicate where the positive or negative charge of the system is concentrated.[26] Table II compares the VDD charges and the electronegativity differences ($\Delta\chi=\chi_{X,A,Y}-\chi_H$) according to Ref. 27. The electronegativity increases with increasing group number and is lower for elements of the third and fourth period than for elements of the second period. Therefore, according to the electronegativity difference $\Delta\chi$, there should be more negative charge (less positive charge) on the hydrogen atoms in the systems with central atoms of the third and fourth periods as compared to the second. Among the central atoms of the considered tetrahedral compounds, nitrogen is the most electronegative element, while aluminum and gallium are the least electronegative elements.

The calculated VDD charges in Table II are in accordance with estimates based on the $\Delta\chi$ values. In each column the hydrogens become more negative when going from the second period to lower periods. In the neutral systems (middle column) the $\Delta\chi$ changes from positive to negative, and indeed the VDD charges show a small charge flux from the hydrogen atoms to the carbon atom in CH_4 upon bond formation, while the opposite holds for SiH_4 and GeH_4. In the negatively charged XH_4^- systems most of the negative charge ends up on the hydrogen atoms, which are much more negatively charged than in the neutral systems. In spite of the overall negative charge, aluminum and gallium still carry positive charges, in agreement with Al and Ga being the least electronegative elements of this set, cf. the large and negative $\Delta\chi$ values for those elements. In the positively charged YH_4^+ systems all the positive charge is located on the hydrogen atoms in the ammonium ion. In spite of the overall positive charge N is slightly negative, in agreement with the large electronegativity of N (cf. the large positive $\Delta\chi$ for N). The positive charge is more evenly distributed in the corresponding ions with arsenic and phosphorus as central atom, in accordance with the much smaller electronegativity of the heavier atoms. We observe that the charge analysis indicates

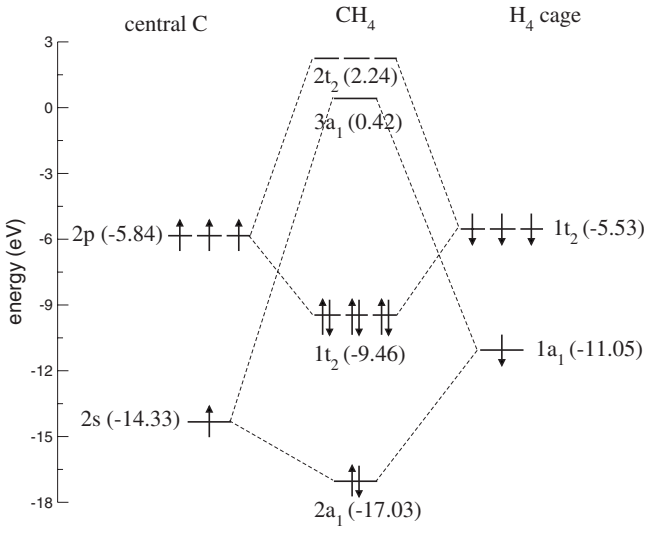

FIG. 1. MO interaction diagram of CH_4. The molecule was divided into two fragments: central C atom and outer H_4 cage. The orbital energies are given in eV.

the most covalent character of the A–H bonds going to the right and down in the periodic system (P and As have the most covalent bonds, but also B and C do not have very polar bonds). Going from the left and down (Ga, Al) to the right and up (N) one recognizes the most polar bonds, with opposite polarity for Ga and N.

The bonds are analyzed in the framework of the Kohn-Sham molecular-orbital model using the fragment approach (FA); see Ref. 28. For this purpose, the XH_4^- (X=B,Al,Ga), AH_4 (A=C,Si,Ge), and YH_4^+ (Y=N,P,As) molecules were divided into two fragments: the central X, A, and Y atoms and the outer H_4 cage. A spin-up sp^3 valence electronic configuration was enforced on the central atoms, and the equivalent spin-down configuration on the H_4 cage (see the CH_4 example of Fig. 1). With this choice of valence configuration of the fragments, the H_4 cage is always neutral and the central atom is either neutral (C,Si,Ge), positive (N,P,As), or negative (B,Al,Ga). A method of quantifying the ionic versus covalent character of electron-pair bonds is to use the composition of the MOs of the compound system in terms of the percentage character of the singly occupied molecular orbitals (SOMOs) of each fragment.[29] According to this approach, a bond is purely covalent if the unpaired electrons of both fragments pair up in an electron-pair bonding orbital with equal contributions from both fragment SOMOs. A bond is purely ionic if the unpaired electron of one fragment is completely transferred to the other fragment forming a lone-pair-like MO in the full system (100% composed of one fragment SOMO, but now occupied with two electrons). This method requires percentage character of a MO in terms of fragment orbitals, which is obtained with a classical Mulliken type analysis of a single MO density in terms of fragment orbital contributions. Such a Mulliken analysis only yields reliable results for small basis sets.[26] The SOMO Mulliken populations could become unrealistic for basis sets containing diffuse functions since such functions on a given atom can in fact describe the electron density on neighboring atoms. Thus, we use here the DZ basis set for the purpose of the SOMO analysis, in order to remove all the spurious effects of the diffuse and polarization functions. As shown for CH_4 in Fig. 1, the electron-pair bonding MOs of the considered molecules have A_1 or T_2 symmetry. The A_1 and T_2 bonds that result do not necessarily have the same degree of ionicity. Whereas the atomic charge analysis only reflects the overall situation, the SOMO population analysis reveals the character of the two types of bond. Table III shows the contributions of the fragment SOMOs for all the considered XH_4^-, AH_4, and YH_4^+ molecules. Clearly, within the considered molecules of the second period (BH_4^-, CH_4, NH_4^+), the B–H bond in BH_4 is the most covalent one, both the A_1 and T_2 bonds being almost purely covalent. Moving to the right in the second period, both the A_1 and T_2 bonds become increasingly ionic, in keeping with the increasing electronegativity of the central atom. In fact, the bonds in NH_4^+ are the most ionic (76% and 70%) within the whole set of molecules, but also the bonds in CH_4 are, contrary to popular belief, not strictly covalent, with 66% and 59% C character in A_1 and T_2, respectively. When one goes down in a group to the third and fourth period, the bonds become less covalent in group 3 (B,Al,Ga), but the A_1 and T_2 bonds develop opposite polarity. The T_2 bonding orbitals in GaH_4^- are polarized toward the H's, and since there are three of them and there is only one A_1 bonding orbital polarized toward Ga, the net effect is the polarization toward the hydrogens that we observed in the charge distribution. For Si and Ge the T_2 are slightly polarized toward the hydrogens (less so than for less electronegative Ga/Al) but these bonds remain reasonably covalent. However, the A_1 orbital is rather polarized toward the central atom. The three T_2 orbitals still cause the total charge to be very slightly negative on the hydrogens. In the group 5 molecules the larger electronegativity of the central atom causes all bonds to be polarized toward Y, of course the most extreme in the case of N. In general, the comparison between the third and fourth period molecules does not show any major differences, in agreement with the VDD and $\Delta\chi$ values of Table II. The AlH_4^- molecule[30] has received some attention, in view of the importance of alanates in the hydrogen storage problem, but the nature of the Al–H bond has remained controversial, the Al–H bond being described as either ionic[31] or covalent[32] (but "highly ionic" covalent) in $NaAlH_4$. The AlH_4^- bond character as it emerges from our analysis is rather ionic (ca. 70%) in the most important (highest lying) set of T_2 bonding orbitals. Although the bond

TABLE III. SOMO contributions to the electron-pair bonding MOs of A_1 and T_2 symmetry in XH_4^- (X=B,Al,Ga), AH_4 (A=C,Si,Ge), and YH_4^+ (Y=N,P,As).

		X/H_4		A/H_4		Y/H_4
A_1	B	51/49	C	66/33	N	76/22
	Al	57/43	Si	72/28	P	79/20
	Ga	66/34	Ge	77/23	As	83/16
T_2	B	43/55	C	59/40	N	70/26
	Al	26/70	Si	41/56	P	54/42
	Ga	30/66	Ge	44/53	As	57/39

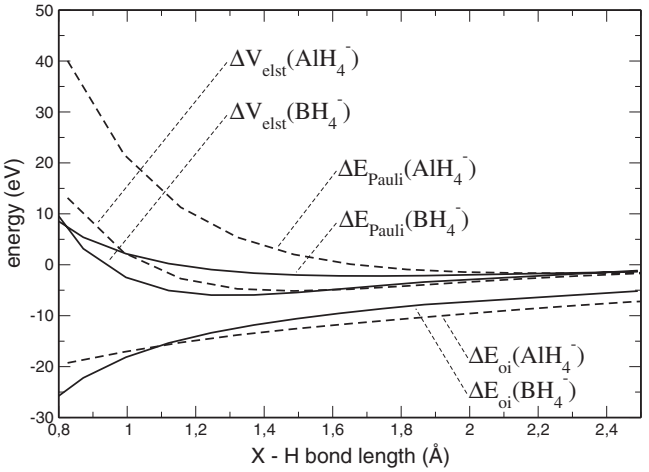

FIG. 2. Comparison between BH_4^- and AlH_4^- bond energy decomposition.

is much more covalent in its A_1 component, the T_2 bonding orbitals predominate, also in the total charge distribution.

B. Bond energy analysis

In the framework of Kohn-Sham MO theory in conjunction with the fragment approach, one can decompose the bond energy in contributions associated with the various orbital and electrostatic interactions. We analyzed the *X*–H, *A*–H, and *Y*–H bond energies following a Morokuma-Ziegler type energy decomposition[33–36] as implemented in ADF. The interaction energy between the fragments is divided into electrostatic interaction, Pauli repulsion (or exchange repulsion), and (attractive) orbital interaction [Eq. (2), below].

$$\Delta E_{\text{int}} = \Delta V_{\text{elst}} + \Delta E_{\text{Pauli}} + \Delta E_{\text{oi}}. \tag{2}$$

The term ΔV_{elst} corresponds to the classical electrostatic interaction between the unperturbed charge distributions of the prepared fragments and is usually attractive. Prepared means: deformed from equilibrium geometry to actual geometry in the overall system and put in the "valence configuration." In the present case this means that the central atoms are excited to the sp^3 configuration, and fully spin polarized, and the H_4 cages are formed from four isolated H atoms, in $(a_1)^1(t_2)^3$ configuration, again with full—opposite—spin polarization. The Pauli repulsion (ΔE_{Pauli}) comprises the destabilizing interaction between occupied orbitals and is responsible for the steric repulsion. The orbital interaction ΔE_{oi} accounts for both the electron-pair bonding between SOMOs on the fragments, and donor-acceptor interactions between occupied orbitals on one fragment with unoccupied orbitals of the other. In addition it contains the effect of polarization (empty-occupied orbital mixing on one fragment due to the presence of another fragment).

Figure 2 shows the results of the bond energy decomposition obtained for BH_4^- and AlH_4^- at different *X*–H bond lengths. The difference between AlH_4^- and GaH_4^- was found to be negligible, as expected from the VDD and SOMO analysis of Sec. III A. A comparison between BH_4^- and AlH_4^- (or GaH_4^-) reveals that, for any fixed *X*–H bond length

TABLE IV. *X*–H, *A*–H, and *Y*–H bond lengths (Å) of the corresponding XH_4^-, AH_4, and YH_4^+ molecules.

BH_4^-	1.245	CH_4	1.096	NH_4^+	1.030
AlH_4^-	1.652	SiH_4	1.491	PH_4^+	1.409
GaH_4^-	1.623	GeH_4	1.538	AsH_4^+	1.498

smaller than 1.5 Å, the Pauli repulsion (ΔE_{Pauli}) is much stronger in AlH_4^- than in BH_4^-, while the electrostatic (ΔV_{elst}) and orbital-interaction (ΔE_{oi}) energies show much smaller differences. The large difference in the Pauli repulsion between BH_4^- and AlH_4^- is explained by the absence of any subvalence closed *p* shell in the B atom, in contrast with Al (or Ga). In BH_4^-, the ΔE_{Pauli} contribution only originates from the repulsion between the spin-down 1*s* state of the B atom and the four spin-down states of the H_4 (compare Fig. 1). The increase in the Pauli repulsion of AlH_4^- (or GaH_4^-) as compared to BH_4^- shown in Fig. 2 thus results from the repulsive interaction between the spin-down *p* states of the Al (or Ga) atom and the spin-down states of the H_4 cage. The large Pauli repulsion for second and third row elements is a general phenomenon, caused by the larger core. This is reflected by the shorter equilibrium bond length and the larger bond energy in B–H as compared to Al–H (see Table IV and Fig. 3, respectively). Similar results were obtained in the AH_4 and YH_4^+ series. BH_4^-, CH_4, and NH_4^+ are the molecules with the strongest bonds among the ones considered here. Thus, the atomic shell structure effects cause these second row compounds to be the most stable building blocks for III-V solid-state materials for hydrogen storage at room temperature.

IV. XH_4YH_4 SOLID-STATE MATERIALS

A. Net site charges

Let us now extend the molecular studies of Secs. III A and III B to the XH_4YH_4 materials. From now on, we label

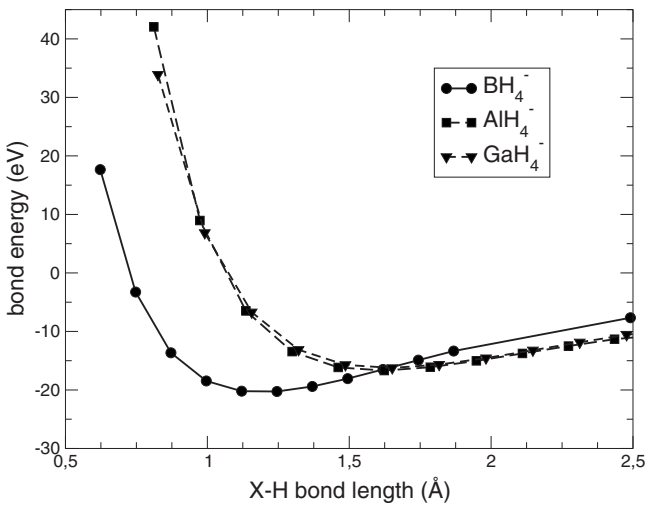

FIG. 3. BH_4^-, AlH_4^-, and GaH_4^- bond energies for different *X*–H bond lengths.

TABLE V. Calculated charges of the XH_4 and YH_4 basic constituents at equilibrium geometry of the corresponding $[XH_4][YH_4]$ material (PBE functional, a.u.).

	XH_4/NH_4		XH_4/PH_4		XH_4/AsH_4
$[BH_4][NH_4]$	−0.83/+1.04	$[BH_4][PH_4]$	−0.85/+1.15	$[BH_4][AsH_4]$	−0.85/+1.10
$[AlH_4^-][NH_4]$	−0.82/+1.03	$[AlH_4][PH_4]$	−0.83/+1.18	$[AlH_4][AsH_4]$	−0.81/+1.16
$[GaH_4][NH_4]$	−0.85/+0.99	$[GaH_4][PH_4]$	−0.86/+1.15	$[GaH_4][AsH_4]$	−0.84/+1.18

them $[XH_4][YH_4]$ to distinguish the condensed materials from the molecular compounds. Until now only ammonium borohydride has been synthesized among the III-V $[XH_4][YH_4]$ materials considered in this paper. It is likely that they are composed of periodic arrays of XH_4 (X=B, Al, Ga) and YH_4 (Y=N, P, As) molecules but the symmetry group is unknown. Thus, we investigated the most common salt lattices: NaCl, CsCl, wurtzite, and zinc blende. The NaCl, CsCl, and zinc blende configurations showed only minor differences in the population analysis, thus only the NaCl results will be reported in the following. The wurtzite configuration was found to be highly unstable, and will not be further considered.

We have determined the net site charges of the XH_4 and YH_4 constituents in the condensed state using a Löwdin population analysis[37] employing a minimal atomic-orbital basis as implemented in ESPRESSO.[15] This charge analysis uses a projection of the plane-wave Bloch states on the minimal basis of AOs (transformed to a Bloch orbital basis). The AOs are optimized so as to minimize the "spillover" of the PW states beyond the space spanned by the AO basis.[38] Still, the incomplete representation of the plane-wave one-electron states by the minimal AO basis leads to an incomplete representation of the charge, which causes the deviation of the sum of the calculated charges per unit cell from zero. This does not imply that the electron density used in the self-consistent calculations would not be properly normalized, it is just an artifact of the projection onto a minimal AO basis.[38] Table V shows the charges of the XH_4 and YH_4 basic constituents at equilibrium configuration of the corresponding III-V $[XH_4][YH_4]$ materials. Although this type of charge analysis does not lead to zero net charge, it does qualitatively indicate the charge distribution in the systems. The calculated charges indeed reflect the expected charge distributions with close to −1 and +1 charges on the XH_4 and YH_4 molecular structure units. The material is in fact an ionic solid consisting of periodic arrays of XH_4^- and YH_4^+ molecular ions.

Figure 4 shows the calculated X–H and Y–H bond lengths for various lattice parameters for $[BH_4][NH_4]$. When the solid is strongly compressed, the B–H and N–H bond lengths in the solid state (full lines) become short, but at the equilibrium value of 6.67 Å (vertical line) they have already closely approached the values for the isolated BH_4^- and NH_4^+ molecular ions (dashed horizontal lines). Apparently, the ions BH_4^- and NH_4^+ constituting this material are virtually identical to their molecular counterparts. Similar results were obtained for all the III-V $[XH_4][YH_4]$ materials considered in this paper, which all exhibit the same strong ionic character.

The molecular calculations are thus consistent with the solid-state results. The bond analysis performed on XH_4^- and YH_4^+ ions keeps its validity in the corresponding $[XH_4][YH_4]$ solid-state materials.

B. Bulk cohesive energies

The cohesive energies of the $[XH_4][YH_4]$ materials were calculated for the NaCl, CsCl, and zinc blende structures according to[39]

$$E_{\mathrm{coh}} = E_{\mathrm{bulk}} - \sum_i E_i, \tag{3}$$

where E_{bulk} is the energy in the $[XH_4][YH_4]$ equilibrium configuration and i runs over the basic constituents of the materials. Isolated atoms are usually considered in the estimation of the cohesive energy, but this choice is not mandatory. As shown before, $[XH_4][YH_4]$ materials consist of periodic arrays of molecular XH_4^- anions and YH_4^+ cations, which we thus consider as the basic constituents in our calculations. We then have to calculate the reference energy of a "bare" anion or cation. In order to perform this calculation with the same plane-wave basis and the same pseudopotential and other approximations, this calculation is performed for a periodic array of such ions in very large unit cells (lattice parameter fixed at 22 a.u. in our calculations), one ion per unit cell. When dealing with charged systems within periodic boundary conditions, one has to pay attention to the problem that the Coulomb energy is divergent if the repeated unit cell carries a net charge. This difficulty can be overcome by in-

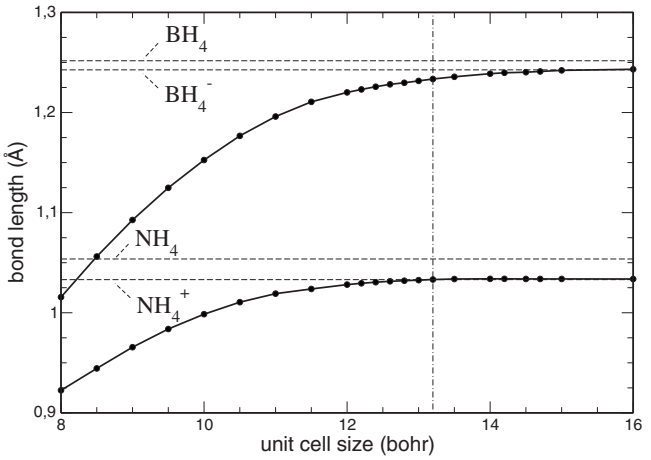

FIG. 4. B–H and N–H bond lengths of crystalline $[BH_4][NH_4]$ for various lattice parameters. The vertical line indicates the equilibrium value of 6.67 Å. The dashed horizontal lines indicate the B–H and N–H equilibrium bond length of the isolated BH_4, BH_4^-, NH_4 and NH_4^+ molecules.

TABLE VI. $[XH_4][YH_4]$ cohesive energies (eV), see Eq. (3) (eV).

	LDA				GGA		
	NH_4^+	PH_4^+	AsH_4^+		NH_4^+	PH_4^+	AsH_4^+
BH_4^-	−7.315	−6.827	−6.772	BH_4^-	−6.594	−5.883	−5.782
AlH_4^-	−7.266	−6.722	−6.686	AlH_4^-	−6.206	−5.609	−5.554
GaH_4^-	−7.322	−6.736	−6.691	GaH_4^-	−6.314	−5.682	−5.638

troducing a uniform background of charge density that exactly compensates the net charge of the unit cell. The problem of calculating the Coulomb energy of a periodically repeating array of charges in a neutralizing background has been widely discussed in the literature. The dominant correction to the energy difference is due to the Coulomb interaction between the charges that, when the repeated unit cell is very large, can be treated by a macroscopic approximation. All energies must be corrected according to the formula proposed by Gillan,[40,41]

$$G_c = \frac{1}{2}\alpha\frac{Q^2}{\epsilon_0 L}, \tag{4}$$

where α is the Madelung constant determined by the lattice, Q and L are the total charge and cell size (22 a.u.), respectively, and ϵ_0 is the dielectric constant of the material.

For the considered $[XH_4][YH_4]$ materials we obtained very similar cohesive energies for the NaCl, CsCl, and zinc blende configurations, with a small preference for NaCl as compared to CsCl (0.05 eV higher) and zinc blende (0.12 eV higher). It is well known that the LDA overestimates the binding energy and underestimate the bond length by 1–2%. The GGA tends to improve upon the LDA in many aspects, especially for atomic energies and structural properties. However, the GGA typically overestimates the bond length by about 1%. Overbinding in LDA results in underestimation of the lattice constant and overestimation of the bulk modulus and cohesive energy. Underbinding in the GGA results in overestimation of the lattice constant and underestimation of the bulk modulus but generally provides more accurate results than the LDA. Table VI shows the calculated LDA and GGA cohesive energies for the NaCl configuration. The ammonium borohydride exhibits the highest values among all possible combinations. Along the series of cations the trend is toward a larger cohesive energy for $N: NH_4^+ > AsH_4^+ \approx PH_4^+$. This holds for each anion, and both for LDA and GGA (PBE). The variation is smaller along the anions, but again the largest cohesive energy is always for the lightest element, and in most cases the largest step is again from third period to the second: $BH_4^- > AlH_4^- \approx GaH_4^-$. In fact, in all cases the cohesive energy becomes a bit lower in going from GaH_4^- to AlH_4^-, and then becomes clearly larger again for BH_4^-. These trends follow the trends in the distance from the X to the Y nucleus, these distances being clearly shortest for the materials with second period hydrides involved. Table VII shows the calculated X-Y distances between the central X and Y atoms of the basic XH_4^- and YH_4^+ constituents of the $[XH_4][YH_4]$ ionic compounds for the NaCl configuration.

TABLE VII. X-Y distances between the central atoms of the molecular XH_4^- and YH_4^+ constituents of the $[XH_4][YH_4]$ ionic salts (Å).

	LDA				GGA		
	NH_4	PH_4	AsH_4		NH_4	PH_4	AsH_4
BH_4	3.34	3.70	3.71	BH_4	3.49	3.84	3.89
AlH_4	3.57	3.89	3.97	AlH_4	3.76	4.23	4.24
GaH_4	3.49	3.84	3.89	GaH_4	3.76	4.24	4.24

The trends can then be explained as a result of the trends in the Madelung contribution. As highlighted in Sec. IV A, the molecular XH_4^- anions (X=B,Al,Ga) and YH_4^+ cations (Y=N,P,As) always carry an almost integer net site charge, the Madelung electrostatic interaction between the two arrays being responsible for the stability of the $[XH_4][YH_4]$ ionic crystals. Due to a larger electrostatic interaction between the XH_4^- and YH_4^+ arrays for a shorter X-Y distance, a higher cohesive energy of the $[XH_4][YH_4]$ material is obtained for the cases with one second period hydride, and the highest cohesive energy when both the anion and the cation are from the second period, i.e., for $[BH_4][NH_4]$.

C. Hydrogen desorption

To this day, there is still a debate about the decomposition products of ammonium borohydride following exposure to ambient conditions. Gutowski and Autrey[6] claimed that $[BH_4][NH_4]$ decomposes into diammonate of diborane (DADB) rather than the BH_3NH_3 polymer. Unfortunately, the bulk structure of DADB has still not been fully clarified and the results should be handled with care. We examined the thermodynamical stability of the $[XH_4][YH_4]$ ionic materials according to

$$[XH_4][YH_4]_{sol} \rightarrow XH_3YH_3 + H_2. \tag{5}$$

The decomposition proposed in Eq. (5), with release of hydrogen and a molecule of XH_3YH_3 per unit cell of the solid, is the simplest choice for the products of the hydrogen release reaction, and is used to provide some energetic results (see Table VIII), leaving aside the possible reaction mechanisms. Again, we found little differences between the three considered crystal structures and only the NaCl results are

TABLE VIII. Hydrogen release energies (eV) according to Eq. (5). Positive values indicate endothermic reaction.

	LDA				GGA		
	NH_3	PH_3	AsH_3		NH_3	PH_3	AsH_3
BH_3	+1.067	−0.363	−0.439	BH_3	+0.243	−1.033	−1.193
AlH_3	+0.744	−0.155	−0.503	AlH_3	−0.194	−0.547	−1.356
GaH_3	+0.952	−0.299	−0.618	GaH_3	+0.101	−1.160	−1.509

reported. On the other hand, we found large differences between the different compounds. For $[BH_4][NH_4]$ at the GGA level (PBE), the hydrogen release is endothermic by 0.24 eV. This is an interesting result, this value being in the desired order of magnitude for viable hydrogen storage materials. It is not a conclusive result, of course, in view of the uncertainty in the DFT calculation, and the neglect of all temperature and entropic effects. It is known that this compound decomposes slowly at room temperature.[5] However, our main goal is to determine if other compounds would be (more) suitable. Judging from the results in Table VIII, most of the other X/Y combinations would yield definitely unstable compounds, with exothermicities for reaction (5) of over 1 eV. Only the other two NH_4^+ salts have small exo- or endothermicities, but they seem to be less stable than $[BH_4][NH_4]$. For each of the anions, BH_4^-, AlH_4^-, and GaH_4^-, the decomposition becomes increasingly more exothermic for the heavier period Y atoms in the YH_4^+ cations. Although the trends are similar for LDA and GGA functionals, the absolute values are significantly different, the LDA model as usual showing rather stronger binding.

In Table VIII the ammonium borohydride is found to be the most stable among the considered $[XH_4][YH_4]$ materials which can be explained from the highest $[XH_4][YH_4]$ cohesive energy in $[BH_4][NH_4]$. As highlighted in Secs. IV A and IV B, this is due to the largest Madelung interaction in that case, which in turn is caused by the shortest X–H and Y–H bonds in the BH_4^- and NH_4^+ ions among all the tetrahedral XH_4^- anions and YH_4^+ cations. The short as well as strong X–H and Y–H bonds for X and Y from the second period stem from the smaller Pauli repulsion with the core compared to the heavier atoms with larger cores. The short bonds lead to closer packing of the crystal.

V. CONCLUSIONS

In this paper we analyzed theoretically the $[XH_4][YH_4]$ materials (X=B,Al,Ga, Y=N,P,As) by means of a combined molecular and solid-state approach. The conclusion must be that $[BH_4][NH_4]$ appears to be most suitable as a hydrogen storage material. Its calculated decomposition into H_2 and NH_3BH_3 is endothermic, while all the other calculated materials (except $[NH_4][GaH_4]$) decompose exothermically. Given that experimentally at room temperature $[NH_4][BH_4]$ is already unstable, it appears that our investigation into the heavier congeners of $[NH_4][BH_4]$ as potential hydrogen storage materials leads to the conclusion that these materials are expected to be less suitable. Our investigation has addressed both the electronic structure of the constituent hydrides and the stability (cohesive energy) of the solid material. First, we clarified the bond character of the isolated XH_4^- (X=B,Al,Ga), AH_4 (A=C,Si,Ge), and YH_4^+ (Y=N,P,As) molecules and ions. The X–H and Y–H bonds have contributions from MOs with A_1 and T_2 symmetry. The B–H bond of the BH_4^- ion was found to be the most covalent among the considered systems due to almost equal contributions from the B and H_4 SOMOs to both A_1 and T_2 MOs. The N–H bond of the NH_4^+ ion, on the other hand exhibits an increased ionicity as compared to the slightly ionic CH_4 case. We found that the bond strength significantly decreases with the third and fourth period central atoms if compared to the second period. This we traced to the Pauli repulsion of the H atoms with the closed core p shells of the third and fourth period central atoms. We have noted that the Al–H bonds in the AlH_4^- ion should not be characterized as covalent; they are rather ionic (70% H character in the T_2 orbitals).

We have confirmed the highly ionic nature of the $[XH_4][YH_4]$ solid-state materials. They are composed of periodic arrays of XH_4^- and YH_4^+ ions. The key elements in the stability of the crystal are the almost integer net site charges carried by the two building blocks and the X-Y distance between the central atoms of the molecular anions and cations, which modulates the electrostatic interaction between the two. The cohesive energy of all considered $[XH_4][YH_4]$ materials was found to be lower than that of the reference $[BH_4][NH_4]$, due to their longer X-Y distances and therefore smaller Madelung stabilization. The hypothetical step of forming H_2 and XH_3YH_3 from the XH_4^- and YH_4^+ ions is not so different energetically for the various combinations that it could reverse, for the energetics of release of H_2, the order established by the cohesive energy. We conclude that the second period derived compound is the only one with a calculated endothermic release energy (0.2 eV) that is of the right order of magnitude to be of interest. However, since this compound already slowly decomposes at room temperature, while all the other compounds are more unstable with respect to the analogous products, we have to conclude that they do not seem to constitute viable alternatives. Other types of chemical modification of the interesting $[BH_4][NH_4]$ compound than variation in the central atoms, such as partial substitution of the H's, may be more promising and are worth investigating.

ACKNOWLEDGMENTS

This work was supported by the Netherlands Programme for Sustainable Hydrogen (ACTS-NWO). Computer resources were provided by the VU University and by the National Computer Facilities (NCF) section of the Netherlands' Organization for Scientific Research (NWO).

*filippo.zuliani@corusgroup.com
†agoetz@few.vu.nl
‡guerra@few.vu.nl
§baerends@few.vu.nl

[1] M. Dresselhaus, G. Crabtree, and M. Buchanan, in *Basic Energy Sciences* (Office of Science, U.S. Department of Energy, Washington, D.C., 2003).
[2] R. Coontz and B. Hanson, Science **305**, 957 (2004).

[3] A. Zuttel, P. Wenger, P. Sudan, P. Mauron, and S. Orimo, Mater. Sci. Eng., B **108**, 9 (2004).
[4] M. Felderhoff, C. Weidenthaler, R. von Helmot, and U. Eberle, Phys. Chem. Chem. Phys. **9**, 2643 (2007).
[5] R. W. Parry, D. R. Schultz, and P. R. Girardot, J. Am. Chem. Soc. **80**, 1 (1958).
[6] M. Gutowski and T. Autrey, Prepr. Pap. - Am. Chem. Soc., Div. Fuel Chem. **49**, 275 (2004).
[7] D. A. Dixon and M. Gutowski, J. Phys. Chem. A **109**, 5129 (2005).
[8] G. Wolf, J. Baumann, F. Baitalow, and F. P. Hoffmann, Thermochim. Acta **343**, 19 (2000).
[9] ADF2006, 01, SCM, Theoretical Chemistry, Vrije Universiteit Amsterdam, The Netherlands; http://www.scm.com
[10] E. J. Baerends, D. E. Ellis, and P. Ros, Chem. Phys. **2**, 41 (1973).
[11] C. Fonseca Guerra, J. G. Snijders, G. te Velde, and E. J. Baerends, Theor. Chem. Acc. **99**, 391 (1998).
[12] R. G. Parr, W. Yang, and M. Ernzerhof, *Density-Functional Theory of Atoms and Molecules* (Oxford University Press, London, 1989).
[13] A. D. Becke, Phys. Rev. A **38**, 3098 (1988).
[14] J. P. Perdew, Phys. Rev. B **33**, 8822 (1986).
[15] S. Baroni *et al.*, http://www.pwscf.org
[16] D. M. Ceperley and B. J. Alder, Phys. Rev. Lett. **45**, 566 (1980).
[17] J. P. Perdew and A. Zunger, Phys. Rev. B **23**, 5048 (1981).
[18] N. Troullier and J. L. Martins, Phys. Rev. B **43**, 1993 (1991).
[19] J. P. Perdew, K. Burke, and M. Ernzerhof, Phys. Rev. Lett. **77**, 3865 (1996).
[20] D. Vanderbilt, Phys. Rev. B **41**, 7892 (1990).
[21] D. J. Chadi and M. Cohen, Phys. Rev. B **8**, 5747 (1973).
[22] A. Baldereschi, Phys. Rev. B **7**, 5212 (1973).
[23] H. Monkhorst and J. D. Pack, Phys. Rev. B **13**, 5188 (1976).
[24] C. Elsässer, N. Takeuchi, K. M. Ho, C. T. Chan, P. Braun, and M. Fähnle, J. Phys.: Condens. Matter **2**, 4371 (1990).
[25] K. M. Ho, C. Elsässer, C. T. Chan, and M. Fähnle, J. Phys.: Condens. Matter **4**, 5189 (1992).
[26] C. F. Guerra, J.-W. Handgraaf, E. J. Baerends, and F. M. Bickelhaupt, J. Comput. Chem. **25**, 189 (2004).
[27] L. C. Allen, J. Am. Chem. Soc. **111**, 9003 (1989).
[28] F. M. Bickelhaupt and E. J. Baerends, Rev. Comput. Chem. **15**, 1 (2000).
[29] F. M. Bickelhaupt, M. Solà, and C. F. Guerra, J. Chem. Theory Comput. **2**, 965 (2006).
[30] D. J. Grant and D. A. Dixon, J. Phys. Chem. A **109**, 10138 (2005).
[31] A. Aguayo and D.-J. Singh, Phys. Rev. B **69**, 155103 (2004).
[32] A. Peles, J.-A. Alford, Zhu Ma, Li Yang, and M.-Y. Chou, Phys. Rev. B **70**, 165105 (2004).
[33] T. Ziegler and A. Rauk, Adv. Inorg. Chem. Radiochem. **18**, 1558 (1979).
[34] T. Ziegler and A. Rauk, Adv. Inorg. Chem. Radiochem. **18**, 1755 (1979).
[35] K. Morokuma, J. Chem. Phys. **55**, 1236 (1971).
[36] K. Kitaura and K. Morokuma, Int. J. Quantum Chem. **10**, 325 (1976).
[37] A. Szabo and N. Ostlund, *Modern Quantum Chemistry* (Dover, New York, 1996), p. 153.
[38] D. Sanchez-Portal, E. Artacho, and J. M. Soler, Solid State Commun. **95**, 685 (1995).
[39] J. Andzelm and L. Piela, J. Phys. C **10**, 2269 (1977).
[40] M. Leslie and M. J. Gillan, J. Phys. C **18**, 973 (1985).
[41] G. Makov and M. C. Payne, Phys. Rev. B **51**, 4014 (1995).